

Monoclinic domain populations and enhancement of piezoelectric properties in a PZT single crystal at the morphotropic phase boundary

Krystian Roleder^{1,*}, Andrzej Majchrowski², Iwona Lazar¹, Roger W. Whatmore³, A. Mike Glazer^{4,5},
Dariusz Kajewski¹, Janusz Koperski¹, and Andrzej Soszyński¹


¹*Institute of Physics, University of Silesia, Chorzow, Poland*

²*Institute of Applied Physics, Military University of Technology, Warszawa, Poland*

³*Department of Materials, Faculty of Engineering, Imperial College London, London, United Kingdom*

⁴*Clarendon Laboratory, University of Oxford, Oxford, United Kingdom*

⁵*Department of Physics, University of Warwick, Coventry, United Kingdom*

 (Received 14 December 2021; revised 12 March 2022; accepted 31 March 2022; published 18 April 2022; corrected 29 April 2022)

The origin of the strong piezoelectric phenomenon in $\text{PbZr}_{1-x}\text{Ti}_x\text{O}_3$ (PZT) perovskites still suffers from a lack of complete understanding. It concerns the distinction between the intrinsic and extrinsic mechanisms that govern PZT's piezo activity. These two mechanisms have been investigated in single crystal $\text{PbZr}_{0.54}\text{Ti}_{0.46}\text{O}_3$ at the morphotropic phase boundary. After poling in a DC electric field, the piezoelectric properties were examined on the same crystal by observing piezoelectric resonances to determine the piezoelectric coefficient d_{31} and measuring quasistatic deformation to determine the coefficient d_{33} . The domain populations were investigated during and after poling in a DC electric field. These populations were also investigated as a function of DC fields for strengths similar to those used to measure quasistatic piezoelectric properties for a poled crystal. The experiments indicate that the intrinsic origin of the enhancement of the piezoelectric properties is connected with a change in the population of domains with monoclinic symmetry, in which there is an easy polarization rotation under the action of the electric field.

DOI: [10.1103/PhysRevB.105.144104](https://doi.org/10.1103/PhysRevB.105.144104)

I. INTRODUCTION

The excellent electromechanical properties of the solid solutions of the perovskite $\text{PbZr}_{1-x}\text{Ti}_x\text{O}_3$ (PZT) have made these materials widely used, e.g., in the production of scientific instruments (scanning probe microscopes [1]), in electronics (transducers [2]), medicine (ultrasonography [3]), sport (electroactive vibration damping [4]), and the automotive sector (fuel injection [5]). Even though PZT has been intensively studied for decades, new unique properties continue to be discovered. PZTs are used only in ceramic form, mainly because it is hard to grow large single crystals. Hence, the first phase diagram for PZT solid solutions proposed by Sawaguchi in 1953 was derived only from measurements on ceramics [6]. Even now, nearly seven decades since the system's discovery, very few papers have reported the properties of PZT single crystals [7–11], mainly because of the technical difficulties involved in their growth [12]. Most papers on PZT have been on ceramics with compositions around the morphotropic phase boundary (MPB). This is a complex boundary with the coexistence of ferroelectric rhombohedral, monoclinic, and tetragonal phases. The strong piezoelectric effects found in MPB-composition ceramics have led to the multitude of practical applications mentioned above.

PZT single crystals have the potential to be even more impressive from the perspective of piezoelectric proper-

ties. Recently, sophisticated structural investigations of PZT materials have revealed a highly complex phase diagram. Long-range average rhombohedral and long-range and short-range monoclinic regions coexist for Zr-rich compositions of PZT [13]. The monoclinic ferric phase possesses three structural variants denoted as M_A , M_B , and M_C [14]. In the M_A and M_B phases, the mirror plane is parallel to $\{110\}_p$, (where the subscript “ p ” indicates Miller indices referred to the pseudo cubic perovskite axes) while in the M_C phase, it is parallel to $\{100\}_p$. The M_A , M_B , and M_C phases differ in the direction of spontaneous polarization, which in the M_C phase is along $\langle 0uv \rangle$, in the M_A along $\langle uuv \rangle$ with $u < v$, and in the M_B along $\langle uuv \rangle$ with $u > v$. The monoclinic M_A phase has been considered as being responsible for the high piezo activity in PZT [14]. It was also found that for a $\text{PbZr}_{0.52}\text{Ti}_{0.48}\text{O}_3$ composition, which is at the monoclinic-tetragonal phase boundary, the crystal structure at room temperature shows after poling a clear tendency to adopt monoclinic symmetry [15]. Moreover, it has been demonstrated that changes induced in the unit cell after applying an electric field do not increase either the rhombohedral or the tetragonal strains. A definite elongation is induced along directions associated with the monoclinic distortion [15].

Recently, a coexistence of the monoclinic M_A and M_B phases has been found at room temperature in a $\text{PbZr}_{0.75}\text{Ti}_{0.25}\text{O}_3$ composition from the nominally rhombohedral side of the MPB, also indicating a local polarization rotation in these phases driven by temperature changes [16]. However, PZTs from the other (nominally tetragonal) side of

*Krystian.Roleder@us.edu.pl

the MPB have exhibited monoclinic distortions only at short length scales. It seems that independent of PZT composition, the monoclinic phase—in which polarization rotation is easily realized—appears to be the main actor deciding on the strength of piezoelectric activity.

Until recently, it was theoretically considered that a sufficiently high domain walls density rather than domain movements could explain the high piezoelectric properties [17]. It was argued that it is the symmetry of the domain walls that accounts for the variety of average symmetries observed in the switching of [001]-oriented lead-based relaxor single crystals into the tetragonal phase via a symmetry-improbable M_C phase. It was also stated that for a crystal in the rhombohedral state, the presence of domain walls imparts monoclinic symmetry. Moreover, this symmetry prevails with increasing domain walls density. A crucial conclusion relies on domain walls breaking the crystal symmetry, allowing observation of the monoclinic phases. This should be especially important in high electric field switching [17].

On the other hand, results obtained from a three-dimensional x-ray diffraction intensity distribution study, which enabled the separation of Bragg peaks diffracted from differently oriented domain sets, made it possible to find, in a single $\text{PbZr}_{0.65}\text{Ti}_{0.35}\text{O}_3$ crystal, the contribution of the domain walls motion estimated at 99 pm/V to the total piezoelectric coefficient of 112 pm/V [18]. This means that the mechanisms that govern the piezoelectric phenomena in ABO₃ perovskites remain unresolved.

We think that experiments mainly on single crystals may distinguish the extrinsic and intrinsic contributions to the excellent piezoelectric properties of PZT compounds. A broad description of such excellent properties of $\text{PbZr}_{1-x}\text{Ti}_x\text{O}_3$ single crystals from the MPB region has been reported in Ref. [19]. In this paper, we report the dielectric, piezoelectric, and optical properties of the $\text{PbZr}_{0.54}\text{Ti}_{0.46}\text{O}_3$ single crystal, discussing the origin of extrinsic enhancement of its piezoelectric properties.

II. PZT SINGLE-CRYSTAL GROWTH

The incongruent melting of PbZrO_3 (PZO) and PZT-solid solutions make crystallization of these compounds possible only at temperatures below the temperature of the peritectic phase transition at 1570 °C [20]. Moreover, high growth temperatures lead to a nonstoichiometry of as-grown crystals because of the volatility of PbO. Therefore, the method of choice for crystallization of PZO and PZT is high-temperature solution growth with a self-flux of PbO. This lowers the temperature of PZO crystallization to the 1050–850 °C range. Small amounts of B_2O_3 are usually used to improve crystallization conditions. The melt composition used in our early experiments of PZO spontaneous crystallization was the same as in Ref. [21]: 2.4 mol. % of PbZrO_3 , 77 mol. % of PbO, and 20.6 mol. % of B_2O_3 . During further investigations, it was found that the replacement of PbO by Pb_3O_4 notably improves the optical quality of as-grown PZO single crystals [22]. The positive influence of Pb_3O_4 on the quality of growing PZT crystals is not understood, but the only additional factor in the system is the higher valence of some Pb ions connected with a surplus of oxygen. Although pure Pb_3O_4 decomposes

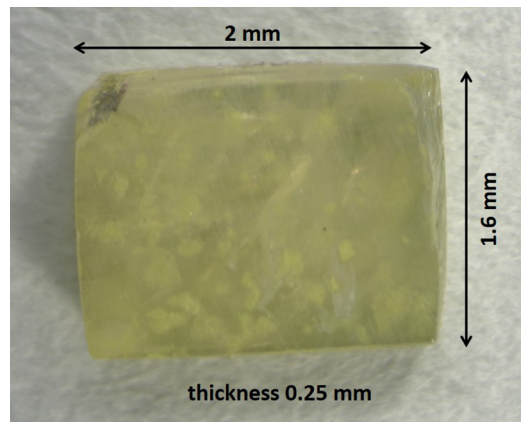


FIG. 1. A single crystal of composition $\text{PbZr}_{0.54}\text{Ti}_{0.46}\text{O}$ obtained by the method described in this paper.

at elevated temperatures, it is thought that some intermediate compounds related to Pb_3O_4 can exist in the flux resulting in the crystallization of totally transparent, colorless PZO single crystals. In our further investigations, it was found that crystallizing PZT compounds is far more difficult than in the case of PZO, mainly as a result of the small distribution coefficient of Ti between the melt and growing PZT crystals. During spontaneous and top seeded solution growth (TSSG) crystallization of PZT from melts of composition used to crystallize PZO (see above), the distribution coefficient k of Ti was near 0.2. Such a small value of k makes it impossible to reach the proper conditions for crystallization of PZT at the MPB composition under the above crystallization parameters. In general, the distribution coefficient depends on the temperature of crystallization, which is connected with the starting composition of the melt. Therefore, starting from the composition mentioned above, we carried out a series of long-lasting crystallization experiments (4 wk each). Both solute concentration in the flux and Ti concentration in the solute were gradually increased. In this way, we could reach an equilibrium crystallization temperature that allowed spontaneous crystallization of PZT crystals with a broad composition range from 20 mol. % of Ti up to MPB. The photograph in Fig. 1 shows a single crystal in the MPB region of composition $\text{PbZr}_{0.54}\text{Ti}_{0.46}\text{O}_3$. The final composition was determined by energy-dispersive x-ray spectroscopy with a precision of $\pm 1\%$. The dielectric properties of this crystal (see below) point to phase transitions that correspond well to those shown in the phase diagram for crystals and ceramics with compositions within the range of the MPB [13,19,23–25].

III. DIELECTRIC AND PIEZOELECTRIC MEASUREMENTS

Samples were coated with silver paste electrodes fired at 750 K for 10 min. Dielectric measurements were conducted using a standard capacitance method. An Agilent 4192A impedance analyzer was used to measure the capacity C and conductance G in parallel circuit mode over the frequency range 1 kHz–1 MHz and at an AC electric-field strength of 0.01 kV/cm. The real part of the complex permittivity was calculated as a ratio of the measured capacity to the capacity

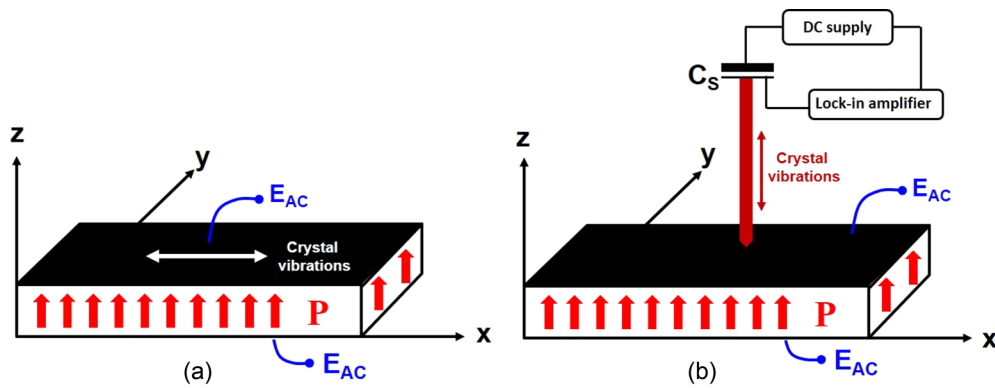


FIG. 2. (a) Sample geometry used to determine the piezoelectric coefficient d_{31} (x , y , and z denote the pseudocubic axis). The black area represents an electrode, and P denotes the resulting direction of polarization in the crystal after poling in a DC electric field. An alternating electric field E_{AC} of the strength of 0.01 kV/cm and frequency in the range 500 kHz–1 MHz was used to measure the piezoelectric resonances. (b) Detection of strain η_3 as a function of electric field E_{AC} of frequency 160 Hz and strength between 0–2 kV/cm. C_S is the sensor capacity to which a DC voltage of the order of 90 V was applied. A lock-in amplifier was used to detect the alternating current, which was proportional to the sample strain η_3 and induced by changes ΔC_S of the sensor capacity (for more details, see the text).

of a vacuum condenser of the same size as the sample. The temperature was controlled using a self-designed temperature controller to a precision on the order of 0.05 K, and measurements were performed at a temperature rate of 1 K/min.

Two methods were used to determine the piezoelectric properties (see Fig. 2). The first employed the Institute of Electrical and Electronic Engineers (IEEE) standard measurements [26,27] of piezoelectric resonances to obtain the piezoelectric coefficient d_{31} . The crystal in Fig. 1 was cut to the shape of a bar $1.75 \times 0.42 \times 0.3$ mm, as in Fig. 2(a), and poled in a DC electric field of 15 kV/cm applied along the $[001]_p$ direction at 340 K, after which the crystal was cooled at 2 K/min under this field, and then switched off at 300 K. The complex admittance Y (magnitude $|Y|$ and phase angle θ) was measured as a function of frequency using the Agilent 4192A impedance analyzer with a sinusoidal voltage of 1V amplitude to find the piezoelectric resonance frequencies. A small frequency step was used to accurately detect the admittance changes near the resonance frequencies. A forced-damped harmonic oscillator model [28] was applied to calculate the elastic compliances, electromechanical coupling coefficient, and low-frequency relative permittivity.

For the same poled sample, the strain η_3 was measured using a quasistatic method based on a capacitance sensor to find the piezoelectric coefficient d_{33} from the relationship $d_{33} = \frac{\partial \eta_3}{\partial E_3}$, where E_3 is the amplitude of the electric field E_{AC} . Details of the measurement method can be found in Ref. [29]. η_3 was induced by an alternating electric field E_{AC} of frequency 160 Hz and amplitude 1.6 kV/cm applied to the sample and transferred via a quartz rod with one end placed on the sample surface. The other end was connected to the plate of a capacitor sensor C_S . The frequency 160 Hz was chosen to minimize external noise and experimental errors. The surface area of the end of the quartz rod touching the crystal was on the order of tens of μm^2 . The field-amplitude increase was automatically controlled and equal to 0.025 kV/cm per minute. Piezoelectric deformation appeared synchronously with the applied voltage frequency ω causing changes ΔC_S of the sensor capacity C_S , according to the time-dependent func-

tion $C_S(t) = C_{S0} + \Delta C_S \sin(\omega t)$. The initial value C_{S0} was adjustable depending on the magnitude of the strain measured, and ΔC_S was determined through recording of the current using a lock-in amplifier, and the piezoelectric strain amplitude η_3 was calculated from $\eta_3 = \frac{\epsilon_0 S}{t_0} \frac{\Delta C_S}{C_S^2}$, where S is the surface area of the sensor capacitance plates, t_0 the thickness of the sample, and ϵ_0 the vacuum permittivity [Fig. 2(b)]. This lock-in technique records the amplitude of the strain exhibited by the sample under the alternating electric field.

IV. EXPERIMENTAL RESULTS

A. Dielectric properties of single $\text{PbZr}_{0.54}\text{Ti}_{0.46}\text{O}_3$ crystal

These properties are determined by temperature changes of the real part of the relative permittivity ϵ'_r in a broad temperature range from 300 to 750 K, for virgin crystal (Fig. 3). The $\epsilon'_r(T)$ runs reach maximal values in the vicinity of 650 K, depending on the frequency. In the phase diagrams mentioned above, this temperature corresponds to the transition to the paraelectric phase for PZT with $x = 0.46$. Moreover, the existence of another transition to the tetragonal ferroelectric phase (near 460 K) is indicated in phase diagram reported in Refs. [23,24]. While in the $\epsilon'_r(T)$ run there is no distinct anomaly at this transformation, the $\epsilon''_r(T)$ does reveal an anomaly at around 460 K.

Figure 3 shows that the temperature of the ϵ'_r maximum shifts towards higher temperature with increasing frequency. There are a number of possible explanations for this dielectric dispersion. It is most probably linked to the motion of complex domain structures. The influence of DC conductivity, which increases with temperature, on the real part of the permittivity cannot be excluded [30], although this seems less likely. The observed dispersion resembles that which occurs in the relaxor-PbTiO₃ solid solutions, which is considered as an indicator of dielectric relaxation attributed to the existence of polar nanoregions [31,32]. One cannot also exclude an influence of a disorder in Pb sublattice, as it was reported in Ref. [33], where first-principle calculations

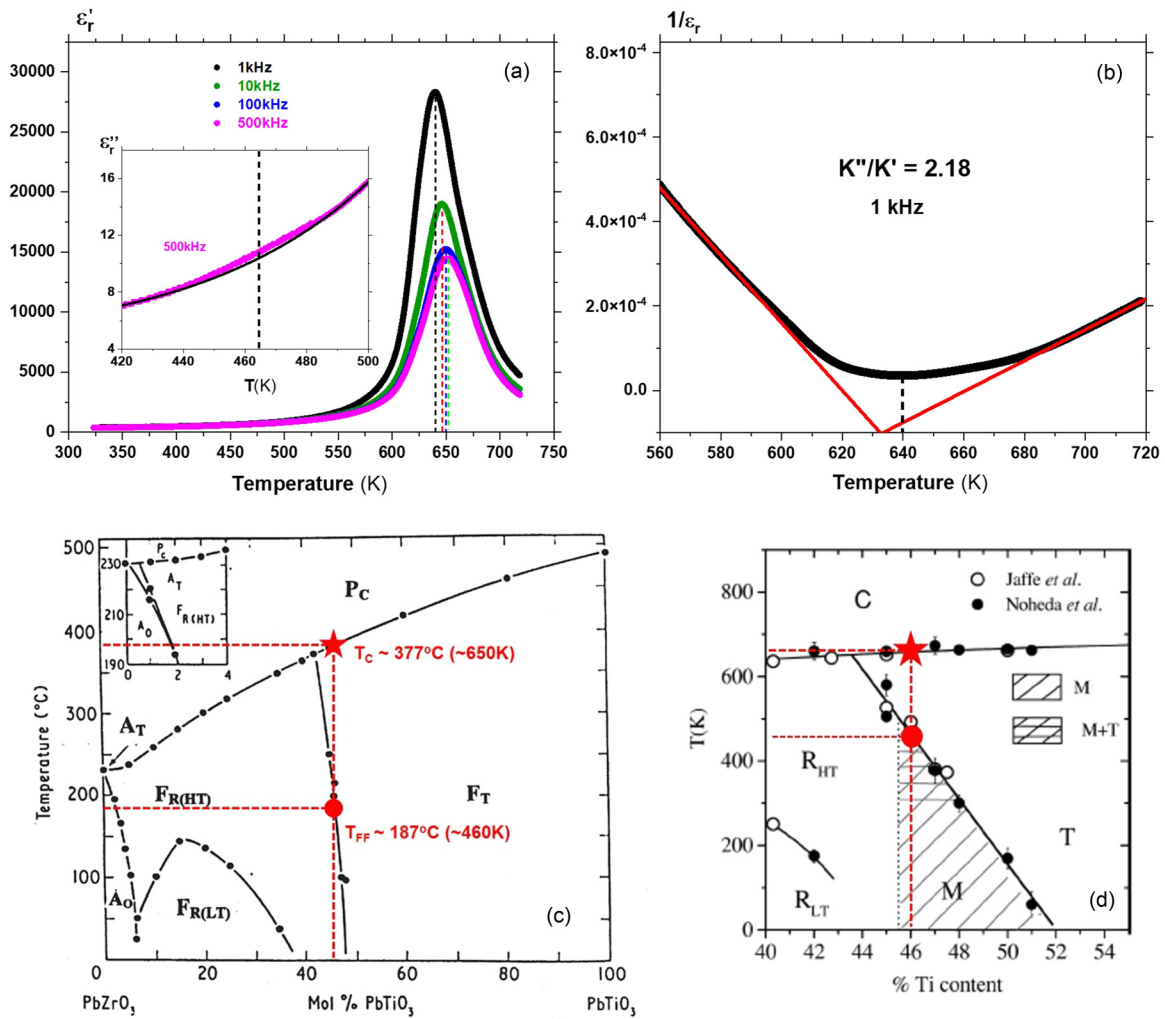


FIG. 3. (a) Temperature and frequency dependence of the real part of the permittivity ϵ_r , near the transition at 650 K (on heating). The inset indicates the existence of another diffuse transition near 460 K on the temperature dependence of the imaginary part ϵ'' of the permittivity (the thin black line is a guide for the eye). (b) The temperature dependences of the inverse permittivities $1/\epsilon'$, measured at 500 kHz, below and above the upper transition, reveal linear functions which allow the Curie-Weiss constants to be calculated. The ratio K'' (below the transition) to K' (above the transition) is very close to that expected for a continuous transition. Also, the minimum value of $1/\epsilon'(T)$, denoted by the dashed line, almost coincides with the point of intersection of straight lines corresponding to the Curie-Weiss law. This intersection does not occur at zero, as predicted by theory. This is connected with the fact that the permittivity does not take, as theory indicates, an infinite value at the transition point. (c), (d) Phase diagrams adapted from Refs. [23,24], on which the chemical composition of the investigated crystal is marked. The transitions depicted by the red stars and circles correspond to those in (a) and (b).

indicated that Pb is differently distorted in relation to the Zr and Ti sublattices in PZT50/50, i.e., in the composition of very similar composition to the investigated crystal. Other possible mechanisms that could cause the dispersion include time-dependent domain walls motion phenomena [34,35] and/or a time-dependent rotation of the polarization under the driving field, which would be linked with the effects on the piezoelectric coefficients discussed below. Further work would be necessary to elucidate which of these effects is responsible. Independently of the above-discussed mechanisms, it appears that the transition at 650 K exhibits a continuous (second-order) phase transition. The ratio of Curie-Weiss constants K' and K'' , respectively, above and below the transition, is dependent on frequency, varying from 2.18 at 1 kHz through 1.90 at 10 kHz, 1.51 at 100 kHz to 1.46 at 500 kHz (see the Supplemental Material for details [36]). This value

should be 2 for a second-order transition, as predicted by the Landau-Ginzburg-Devonshire theory, but measurements have not been made for a single-domain state. Thus, the dielectric response below T_C may be affected by domain structures. These values, the frequency dispersion, and the shape of $\epsilon'(T)$ around T_C point to a phase transition much closer to continuous than discontinuous, with some relaxational character which may be domain related and requires further study. This result corresponds well to the properties of the single crystal of similar composition reported in Ref. [37].

Summarizing this part, we state that the single crystal reveals transition points that correspond to a PZT composition close to the morphotropic phase boundary region. Its dielectric properties show that the crystal undergoes a continuous phase transition near T_C .

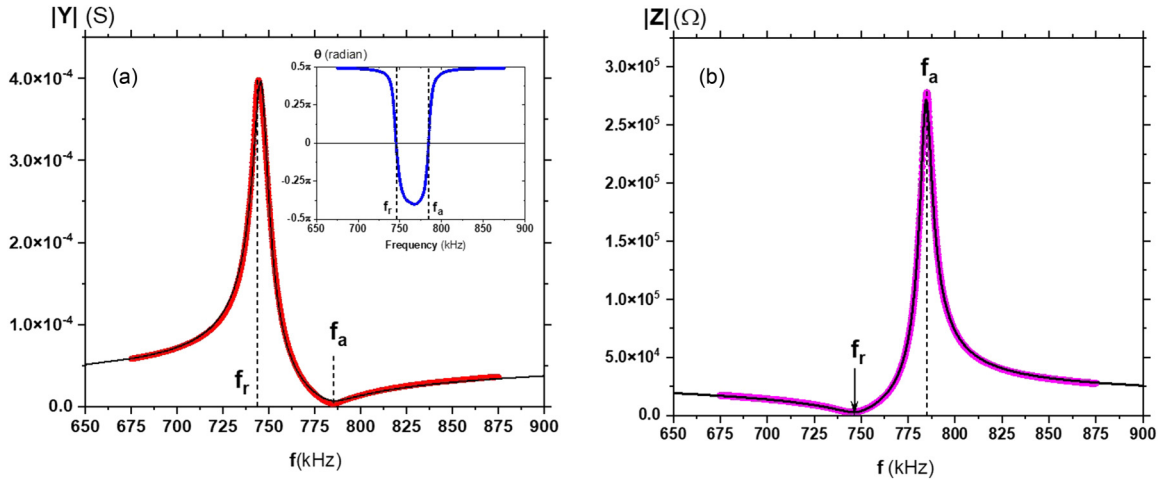


FIG. 4. (a) The modulus $|Y|$ of the complex admittance $\mathbf{Y} = G + iB$ (where G and B are, respectively, the real and imaginary parts of \mathbf{Y}) as a function of frequency at 300 K for a poled single $\text{PbZr}_{0.54}\text{Ti}_{0.46}\text{O}_3$ crystal. The inset shows the dependence of the phase angle θ as a function of frequency f . The maximum and minimum of $|Y|(f)$ corresponds to the resonance f_r and antiresonance f_a frequency, respectively. The black line is a fit for the experimental data. The set of equations [Eq. (1)] was used to fit the $|Y|(f)$ dependence, where $\mathbf{C}_0 = C_0' + iC_0''$ is the low-frequency complex capacitance of the sample, angular frequency $\omega = 2\pi f$. Γ is damping, β is constant, respectively. (b) The modulus $|Z|$ of the complex impedance $\mathbf{Z} = R + iX$ (where R and X are, respectively, the real and imaginary parts of \mathbf{Z}) as a function of frequency at 300 K for a poled single $\text{PbZr}_{0.54}\text{Ti}_{0.46}\text{O}_3$ crystal. The black line gives the experimental data from which the resonance f_r and antiresonance f_a frequencies were determined. The set of equations [Eq. (2)] was used to fit the $|Z|(f)$ dependence, where the angular frequency $\omega = 2\pi f$. Γ is damping, α is a constant, and R_0 is the sample resistivity at low frequency.

B. Piezoelectric properties of single-crystal $\text{PbZr}_{0.54}\text{Ti}_{0.46}\text{O}_3$

The dependence of the $|Y|$, θ and the magnitude of the impedance ($|Z|$) as functions of frequency at constant electric field strength 0.03kV/cm, for a mechanically-free crystal, are shown in Fig. 4. The curves in this figure are characteristic for a crystal in an almost single-domain state, i.e., the function $|Y|(f)$ reaches practically zero for the antiresonance frequency f_a , and the minimum of $\theta(f)$ is very close to -0.5π . Moreover, the theoretically predicted function $|Y|(f)$ fits the experimental points well.

$$G(\omega) = \beta \frac{\omega^2 \Gamma}{(\omega_r^2 - \omega^2)^2 + \omega^2 \Gamma^2} + C_0'' \omega$$

$$B(\omega) = \beta \frac{(\omega_r^2 - \omega^2) \omega}{(\omega_r^2 - \omega^2)^2 + \omega^2 \Gamma^2} + C_0' \omega$$

$$|Y(\omega)| = \sqrt{G^2(\omega) + B^2(\omega)}, \quad (1)$$

$$R(\omega) = \alpha \frac{\Gamma}{(\omega_a^2 - \omega^2)^2 + \omega^2 \Gamma^2} + R_0$$

$$X(\omega) = \alpha \frac{(\omega^2 - \omega_a^2)(\omega - \frac{\omega_r^2}{\omega}) + \Gamma^2}{(\omega_a^2 - \omega^2)^2 + \omega^2 \Gamma^2}$$

$$|Z(\omega)| = \sqrt{R^2(\omega) + X^2(\omega)}. \quad (2)$$

Determination of the piezoelectric coefficient d_{31} was made by fitting the experimentally measured $|Y|(f)$ and $|Z|(f)$ frequency dependences (Fig. 4) to the theory given by the sets of equations in Eq. (1) and Eq. (2), respectively. The $|Z|(f)$ function was chosen because it allows one to find the piezoelectric frequencies from the same experimental

dependence. We determined $f_r = 746.56$ kHz ($\omega_r = 2\pi f_r$) and $f_a = 784.37$ kHz ($\omega_a = 2\pi f_a$) from $|Z|(\omega)$ [Eq. (2)], and permittivity $\epsilon_{33} = 451.1$ along the z direction from $|Y|(\omega)$ [Eq. (1)] containing static value C' [in the $B(\omega)$ function]. The relationships (3)–(5), below, were used to calculate from $|Y|(f)$ the piezoelectric coefficient $d_{31} = 93.4 \pm 0.2$ pm/V, elastic compliance $s'_{11} = 1.8 \times 10^{-11}$ m²/N, and coefficient of electromechanical coupling $k_{31} = 0.34$, taking the theoretical crystal density to be 7.98 g/cm³ [38]:

$$s'_{11} = \frac{1}{4\rho l^2 f_r^2}, \quad (3)$$

$$\tan\left(\frac{\pi f_a}{2f_r}\right) = \frac{k_{31}^2 - 1}{k_{31}^2}, \quad (4)$$

$$d_{31}^2 = \epsilon_0 \epsilon_{33} s'_{11} k_{31}^2. \quad (5)$$

The values obtained are of the same order as for ceramics presented in Ref. [23].

Determination of the coefficient d_{33} was carried out at room temperature according to the quasistatic (160 Hz) procedure described above [Fig. 2(b)], which is well away from the resonance frequencies. The advantage of this approach is that measurements of the piezoelectric coefficients d_{31} and d_{33} are for the same sample and at the same state of sample polarization. It is worth noting that, in the measurement of d_{33} based on the resonance method, different sample shapes would have been needed to be used, and this would have required different polarisation in a DC field. The strain η_3 as a function of increasing and decreasing field amplitude E_3 is shown in Fig. 5.

As Fig. 5 shows, the linear strain amplitude at low electric-field strengths changes smoothly and linearly with the field

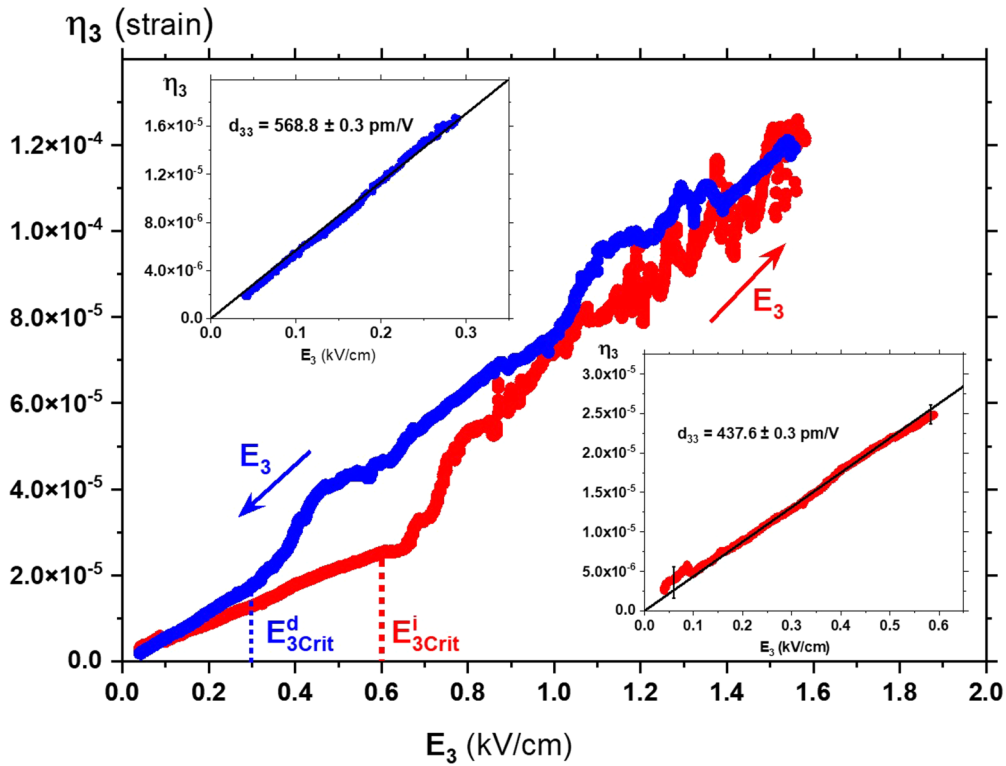


FIG. 5. Quasistatic field-dependent strain η_3 on field increasing (red) and field decreasing (blue) for the same poled single $\text{PbZr}_{0.54}\text{Ti}_{0.46}\text{O}_3$ crystal, for which d_{31} was determined from the observation of piezoelectric resonances. The insets show the $\eta_3(E_3)$ dependence as functions of the AC field amplitude E_3 for which the piezoelectric coefficient d_{33} could be directly determined. The black lines fit the relationship describing the piezoelectric phenomenon $\eta_3 = d_{33}E_3$ (in Voigt notation).

E_3 , independently of the direction of field increase. For these parts of the $\eta_3(E_3)$ runs, the piezoelectric coefficient d_{33} could be calculated. This was equal to about 440 and 570 pm/V for increasing and decreasing fields, respectively. These values are a few times larger than those obtained for d_{31} and are comparable with the values of d_{33} known from the literature (e.g., Refs. [10,17,38,39]). However, there are critical values of E_3 , denoted by $E_{3\text{Crit}}^i$ and $E_{3\text{Crit}}^d$ and the vertical dotted lines in Fig. 5, above which the $\eta_3(E_3)$ dependence becomes irregular, although on average, it remains linear. When the field increases, the critical values are $E_{3\text{Crit}}^i = 0.6$ kV/cm and $E_{3\text{Crit}}^d = 0.3$ kV/cm on the field-decreasing leg. However, this hysteresis is not related in any way to the coercive field because $P(E)$ observed in a Sawyer-Tower setup was linear for all the fields used.

Moreover, it was checked that after these experiments, the $|Y|(f)$ and $\theta(f)$ dependences did not change, and they were the same as that observed after poling the crystal in a DC electric field (See Supplemental Material at [36]). It means that the state of polarization in the sample was not destroyed by the AC field used to measure d_{33} .

It should be stressed that the maximum AC field of 1.6 kV/cm was much smaller than the coercive field (8 to 10 kV/cm), and thus the $P(E)$ run was a linear function during the whole experiment. It also means that the relationships $\eta_3(E_3)$ are reversible, at least for field strengths not exceeding those used in our experiments.

The most unusual effect is an irregular $\eta_3(E_3)$ dependence above $E_{3\text{Crit}}^i$ and $E_{3\text{Crit}}^d$. Interestingly, in the case of strains

detected for increasing E_3 , the irregularities are stronger than for decreasing fields. However, as shown in Fig. 6, also for these irregular parts of $\eta_3(E_3)$, a linear extrapolation closely obeys the piezoelectric relationship $\eta_3 = d_{33}E_3$. It can be said that in this case, we are dealing with an enhancement of the piezoelectric coefficient d_{33} . This increases from 40% (for decreasing field) to 66% (for increasing field) compared with low fields.

As the piezoelectric resonances are unchanged by the quasi-DC strain measurements, this means that the polarization state of the sample was also unchanged under the alternating field cycle. Therefore, the observed irregularities could not have come from domain movements induced by a possible depolarization process while the sample was under the 160 Hz AC electric field. If this had been the case, the polarization would have been considerably smaller, and the piezoelectric resonances would have disappeared or at least become significantly weaker. Also, the quasistatic $P(E)$ dependence would not have been linear. This means that the origin of the enhancement of the piezoelectric properties of single crystal $\text{PbZr}_{0.54}\text{Ti}_{0.46}\text{O}_3$ must be connected with another mechanism. It is known that domain walls can move in low electric fields [40,41]. In such a case, the polarization state of the sample would not be significantly changed because the applied AC field is far below the coercive field. Nevertheless, domain-wall motions can certainly contribute to the jumps in $\eta_3(E_3)$ dependence.

To find the mechanism enhancing the piezoelectric properties, we decided to observe domain behavior during the

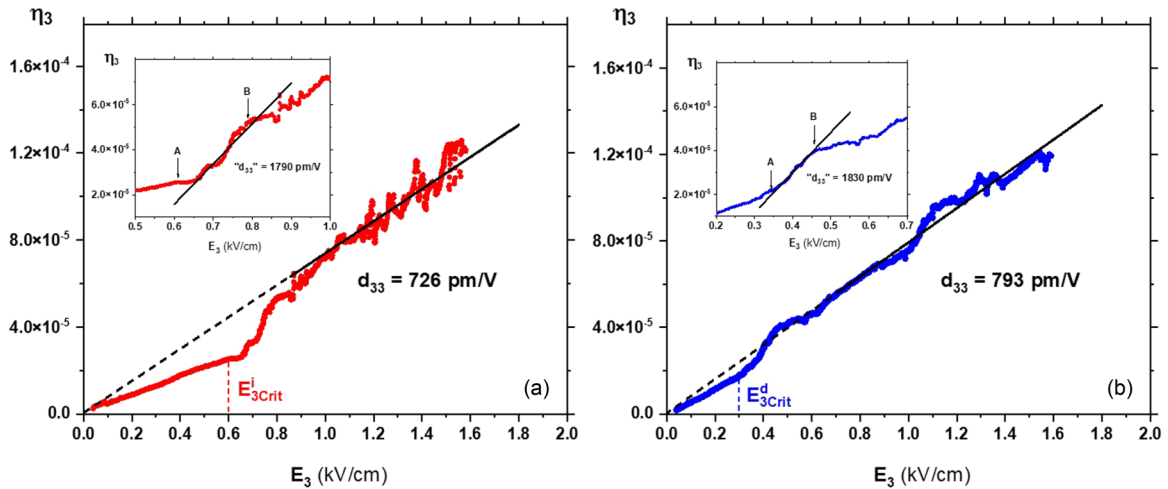


FIG. 6. Fitting the irregular part of the $\eta_3(E_3)$ dependence to the relationship describing the piezoelectric phenomenon $\eta_3 = d_{33}E_3$. These extrapolations give a value of the piezoelectric coefficient d_{33} for increasing (a) and decreasing (b) strength of the electric field E_3 . In both figures (see insets), the A-B transient region can be distinguished, in which the population of the monoclinic phases changes (see Fig. 9 further in the text). Insets in (a) and (b) show that these changes occur in the same way, i.e., slopes of the black lines are almost the same for increasing and decreasing AC field. The slopes correspond to high piezoelectric coefficients denoted as “ d_{33}^d ”.

poling process and their reorganization during the action of DC fields in the range of electric-field strengths at which the high quasistatic piezoelectric properties were detected (Figs. 5 and 6).

C. Optical investigations

To understand the complex piezoelectric response presented in the previous section, we have carried out optical studies of the domain structures of the $\text{PbZr}_{0.54}\text{Ti}_{0.46}\text{O}_3$ single crystal using the Metripol technique [42–44] (See Supplemental Material [36]). This technique measures an orientation angle φ , the extinction angle in polarizing microscopy. A feature of the Metripol is the visualization of optical indicatrix orientations. These orientations are presented as a colored map, in which different colors are related to different angles φ . The empirical distribution of orientations δ_d (histogram) can be plotted based on such maps. Each point of such a histogram corresponds to the orientation distribution calculated for 1° intervals.

Using the experimental technique mentioned above, we have studied the domain structures in the virgin and DC poled $\text{PbZr}_{0.54}\text{Ti}_{0.46}\text{O}_3$ single crystal. The direction of the applied electric field was along with the thickness of the sample, i.e., it was parallel to the incident light path. This electric-field orientation was achieved in a specially prepared capacitor placed in the Linkam stage. This capacitor consisted of two glass plates coated with indium tin oxide forming transparent electrodes. The crystal was placed between these plates to which a constant electric field could be applied using thin silver wires glued to the electrodes. Measurements of the optical properties of the $\text{PbZr}_{0.54}\text{Ti}_{0.46}\text{O}_3$ single crystal were carried out from 300 to 390 K, i.e., the temperature at which the sample was poled in a DC field.

At room temperature, the domain structure in the ferroelectric phase of the virgin crystal is a mixture of domains differently oriented to each other when viewed along $[001]_p$. As can be seen from the PZT phase diagram [Fig. 3(d)], the

structure of the crystal at 300 K consists of a mixture of rhombohedral, monoclinic, and tetragonal phases. However, see Fig. 8 which shows the population of the extinction positions of domains, where there is a continuous change of these

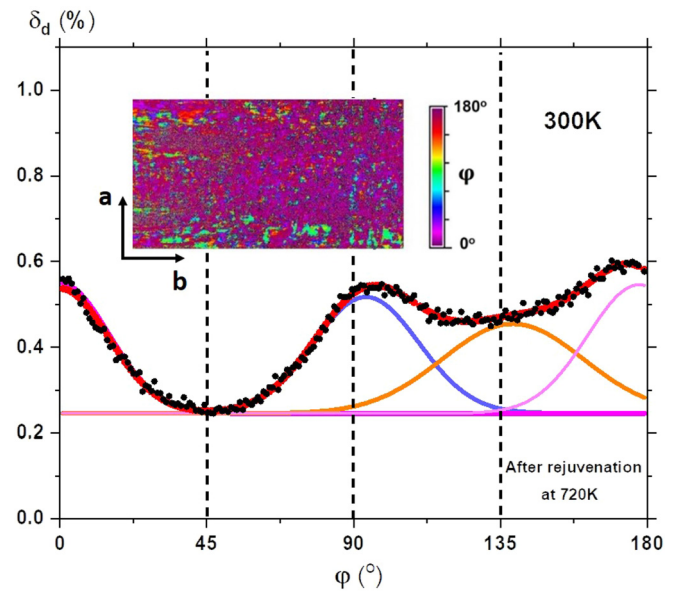


FIG. 7. Domain populations δ_d at 300 K of randomly oriented domains for a crystal annealed at 720 K for 30 min. *a* and *b* denote $(100)_p$ axes (*c* axis is perpendicular to the crystal surface). Continuous Gaussian lines are fits showing extinction angles very close to the tetragonal (0° and 90°) and rhombohedral (135°) symmetries. There is a background in the whole range of angles (a continuous line for each Gaussian line) which originates from numerous domains walls or domains sitting on each other and affects the average optical indicatrix section. Inset is a representative orientation map for a region of $820 \mu\text{m} \times 440 \mu\text{m}$. φ denotes the angle at which the slow axis of the indicatrix is inclined to the horizontal direction. A diagram showing possible excitation orientations for each phase is reported in Ref. [5].

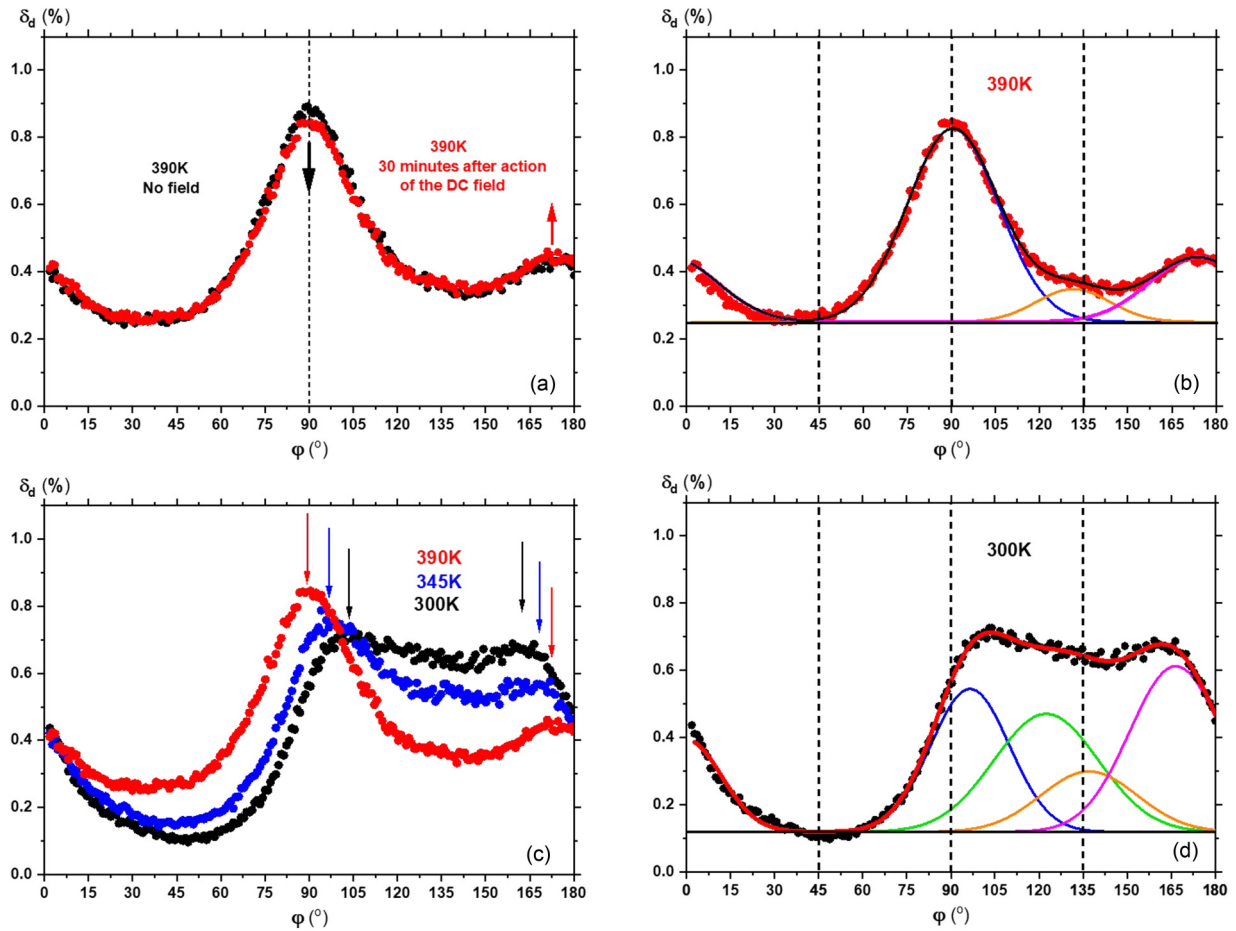


FIG. 8. (a) Domain populations δ_d during poling in a DC electric field of strength 15 kV/cm applied at 390 K. Even after 30 min, the population does not change significantly, with only a tendency to decrease around 90° and increase around 170° . (b) Gaussian lines fitted to the histogram obtained 30 min after the DC electric field was applied at 390 K. These prove the coexistence of tetragonal and rhombohedral optical orientations. (c) Cooling the crystal in the presence of the DC field makes this tendency much stronger and eventually a distinct difference in the distribution of optical orientations at 300 K is seen. This tendency is denoted by arrows showing a shift of local diffuse maxima of populations towards higher and lower angles, respectively. (d) Final distribution of optical orientations after poling process. All Gaussian lines point to monoclinic symmetries of the final state, in which optical orientations of domains can take any orientation different than 90° , 135° , and 180° [10]. Note the distinctly lower background compared to that in (b). The black (b) and red (d) curves are a result of (cumulative) curves.

orientations (the data were fitted with a Gaussian distribution function called Gaussian lines, further in the text). The domains with rhombohedral symmetry with extinction orientations of 45° and 135° correspond to local minima in the two halves of Fig. 7. This diffuse dependence of the domain populations stems from domains of monoclinic symmetry M_A , M_B , and M_C [45], which can also take any orientation, different from the angles 0° , 45° , 90° , 135° , and 180° [10]. As discussed in Ref. [45], the Gaussian lines correspond to the distribution of the optical indicatrix orientations (responsible for extinction directions of domains) characterizing the monoclinic symmetries.

Interestingly, the poling of the crystal does not lead to asymmetric distribution of domain orientations. Figure 8(a) presents changes in time of the domain populations (looking down $[001]_p$) after switching in a DC field of 15 kV/cm, i.e., in the same way that the electroded crystal was poled to induce piezoelectric properties. It is seen that there is no

distinct influence from the DC field applied at 390 K. The population of indicatrix orientations points to a coexistence of the tetragonal and rhombohedral symmetries [Fig. 8(b)]. Only after cooling, in the presence of this field, do the domain populations evolve toward an asymmetric distribution at 300 K, with a different population of indicatrix orientations corresponding to angles distinctly different from 0° and 90° [Figs. 8(c) and 8(d)]. This points to developing populations of domains with monoclinic symmetry, in which the continuous rotation of P_3 in the DC fields can take place [10]. Moreover, the “background” decrease suggests that the poling reduces the population of domain walls.

To find the origin of the high values of the piezoelectric coefficient d_{33} presented in Fig. 6, we carried out measurements of domain populations as a function of the DC electric-field strength for a crystal polarized under the same conditions (the crystal was not electroded). This dependence is shown in Fig. 9, from which it appears that with the DC strength

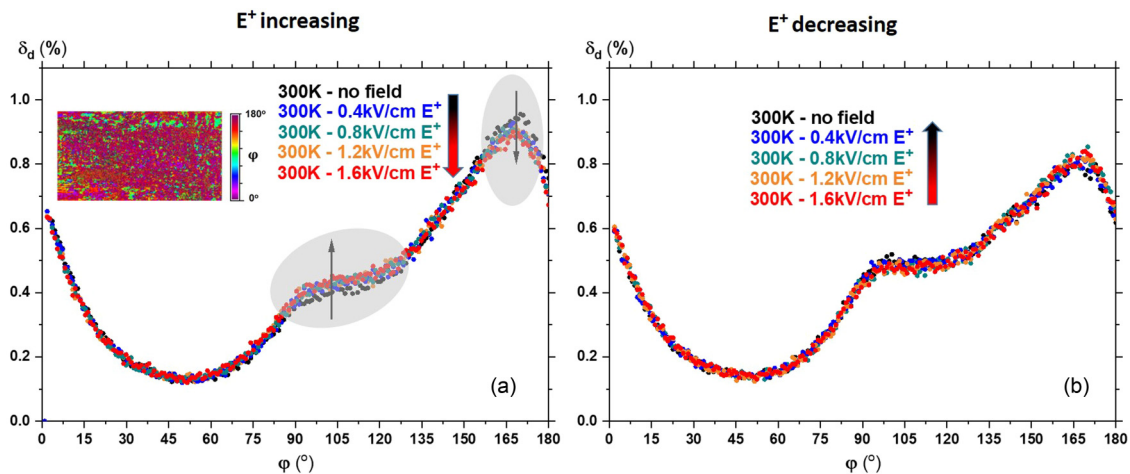


FIG. 9. (a) Changes of domain population δ_d , four days after poling, as a function of the applied DC electric fields of intensities the same as used in AC field (see Figs. 5 and 6). With the increase of this field, many distinct changes take place for orientations greater than 90° . The most sensitive regions to the action of the DC field are shadowed, and black arrows denote the direction of change in population with the increase in the field strength E^+ . The inset is a map of indicatrix orientations at 300 K in the absence of the field. (b) In the case of the decreasing field, the sensitivity of these regions can be neglected, although a discrepancy in experimental points for orientations greater than 90° can be recognized.

(denoted as E^+) increasing, many more orientable domains appear with angles in between 90° and 180° . Moreover, the higher the DC field strength, the population of angles between 90° and 135° increases at a cost in domain populations between 150° and 180° [see Fig. 10(a) with shadowed areas]. With decreasing field E^+ , the population of domains does not change [Fig. 10(b)], although there is a discrepancy in the population between the ranges (0° – 90°) and (90° – 180°).

Moreover, the reorientation process is not symmetric concerning the electric-field direction. With the change of DC field direction of the same field strength, from E^+ to E^- , the distribution of domain orientations is not symmetric. This is visible in Figs. 10(a) and 10(b), representing this effect for the same field strengths as used in measurements of the quasistatic piezoelectric properties (Figs. 5 and 6).

The most prominent result of the optical properties investigations is represented in Fig. 10. Gaussian line fitting shows that the enhancement of the piezoelectric properties is not related to domains of rhombohedral symmetry. These domains are not involved in domain reorientation under an electric field producing a piezoelectric strain [Fig. 10(c)]. This points to the domains of monoclinic symmetry playing an essential role in the enhanced piezoelectric properties demonstrated in Figs. 5 and 6.

V. DISCUSSION

If the domains were purely rhombohedral, with their spontaneous polarizations appearing along the $[111]_p$ direction (with 45° and 135° extinction angles), then after poling, the crystal should be close to being in a state in which the polarization is ordered around the $[001]_p$ axis, i.e., perpendicular to the crystal surface. However, as was previously reported [15], such crystals tend to have monoclinic symmetry after

poling in a DC field. After poling, a complex distribution of the monoclinic (M_A , M_B , and M_C), rhombohedral ($R3m$), and tetragonal ($P4mm$) phases has been observed in the investigated crystal (Figs. 8–10). Classical piezoelectric resonances have been observed (Fig. 4), as generally for a single-domain crystal under a low-strength electric field. Another proof of this permanent state is given by the quasistatic strains induced by low AC electric-field strengths for the same sample and the same polarization state. As shown in the insets in Fig. 5, a smooth $\eta_3(E_3)$ dependence, for low strengths of the field E_3 , is well described by the piezoelectric relationship $\eta_3 = d_{33}E_3$ with piezoelectric coefficient d_{33} , much higher than d_{31} , was observed.

However, the most crucial feature in Figs. 5 and 6 is the $\eta_3(E_3)$ dependence for AC electric fields greater than 0.6 kV/cm. This dependence remains linear, as expected for the piezoelectric effect, and contains strain jumps. They are easily visible with increasing field strength and make the high-field $\eta_3(E_3)$ dependence irregular. It has to be stressed that when the AC field was switched off, the sample revealed the same piezoelectric resonances as those observed before the experiments in AC fields. This proves that the action of this field has not destroyed the resultant polarization state.

Although domain walls movements have a share in the enhancement of the piezoelectric properties, we consider that mainly rotation of the polarisation in the monoclinic phases dominates, as theoretically considered by Ballaiche *et al.* [46]. It also indicates that with the application of an electric field along $[001]_p$ to rhombohedral $\text{PbZr}_{1-x}\text{Ti}_x\text{O}_3$ with $x = 0.47$, i.e., very close to the composition of the crystal investigated by us, both the triclinic and monoclinic M_C symmetries are induced. At the same time, it was found that in the monoclinic structure, significant shear piezoelectric coefficients appear. Hence, a part of the strain η_3 presented in Fig. 6 for fields greater than 0.6 kV/cm corresponds to the piezoelectric

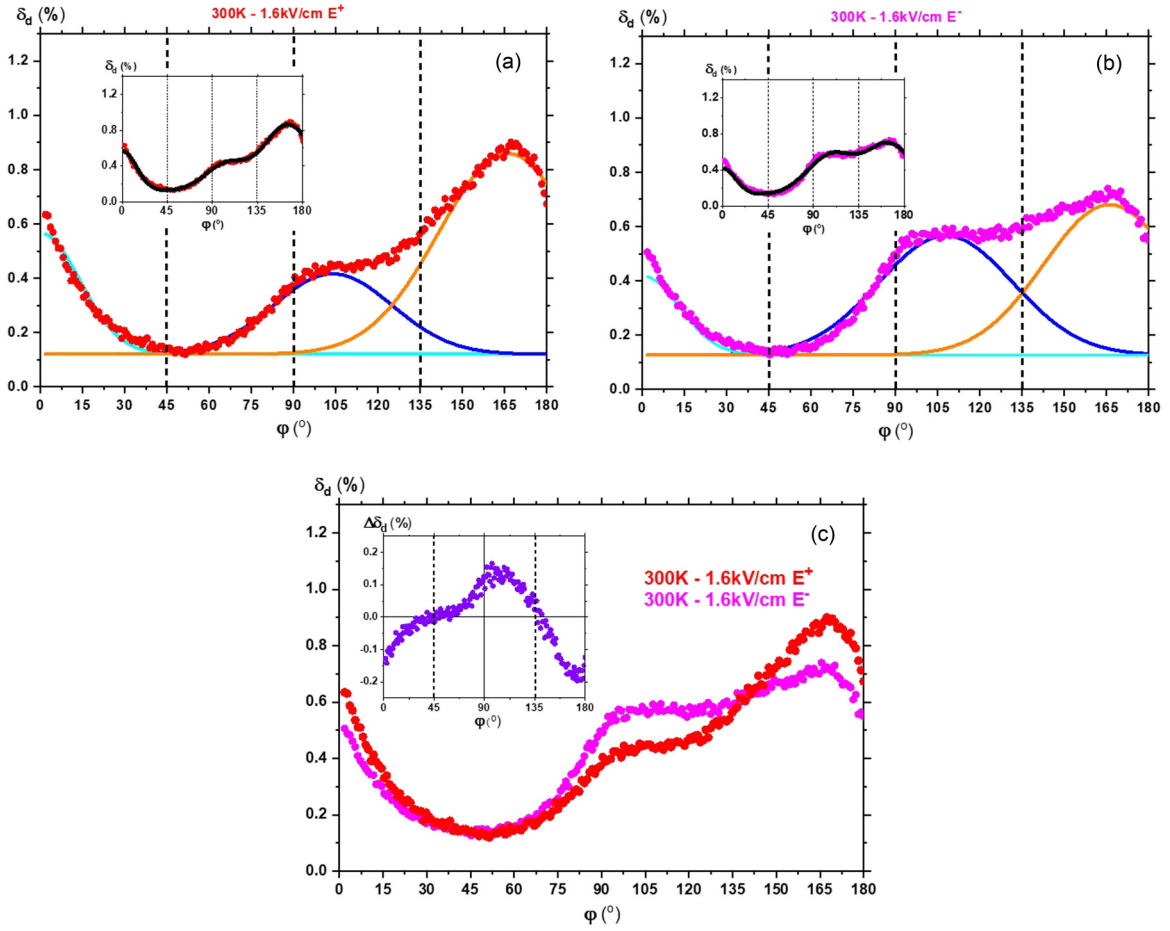


FIG. 10. Fit with Gaussian lines describes the domain populations δ_d : (a) at final electric-field strength, 1.6 kV/cm E^+ and (b) opposite field, 1.6 kV/cm E^- . The action of such a field on the poled crystal leaves the background unchanged while broadening distributions of domains with monoclinic symmetries. The insets present the resulting curves and experimental points. (c) Distribution of the domains for two opposite DC fields denoted E^+ and E^- . Inset shows the difference in domain populations $\Delta\delta_d$ under the action of such fields. Interestingly, these fields do not affect the population of the rhombohedral domains 45° and 135° .

modulus d_{33} and piezoelectric shear coefficients, e.g., d_{15} [28]. In this way, a high piezoelectric response for fields above the A-B area in Fig. 6 can be understandable in the context of a change in the population of regions with monoclinic symmetry in Fig. 9 for the fields with the same values as in Fig. 6.

The observed irregularities (pulses) in the $\eta_3(E_3)$ dependence originate from the irregular rotation of P_S , because of blocking of domains of monoclinic symmetry on crystal defects, or from the internal friction in the crystal caused by this rotation in the presence of neighboring regions with domains of, e.g., the rhombohedral symmetry, which does not react to the DC field [Fig. 10(c)]. If the domain walls have any influence on the piezoelectric response, it manifests itself only in the form of observed irregularities and does not cause any significant enhancement of this response. Interestingly, the strain jumps are much smaller in cycles with decreasing electric fields. Moreover, there is a kind of hysteresis in the $\eta_3(E_3)$ dependence, distinctly seen when region A-B in Fig. 7 is considered. As presented in Figs. 10(a) and 10(b), this is connected with stabilizing the population

of regions with monoclinic symmetries. This stabilization is mainly associated with the pinning of the monoclinic domains by defects (e.g., space charge). The domain-pinning process would be expected to exhibit a relaxation process to approach the prefield-application monoclinic domain population state with a particular time constant. This time constant is longer than the period over which the experiment was made and accounted for the apparent hysteretic behavior in the A-B segments in the strain-field amplitude plots shown in Figs. 7(a) and 7(b).

VI. CONCLUSIONS

Intrinsic and extrinsic mechanisms responsible for the piezoelectric effect in single crystal $\text{PbZr}_{0.54}\text{Ti}_{0.46}\text{O}_3$, of composition near the morphotropic phase boundary, have been considered based on the dielectric, piezoelectric, and optical properties measurements. At room temperature, domains with the tetragonal, rhombohedral, and monoclinic symmetries coexist. However, the monoclinic symmetries dominate after poling in the DC electric field. Changes in domain populations

during poling have been investigated. By combining the investigations of optical properties and quasistatic and dynamic piezoelectric properties of a poled single crystal, it was possible to find that the main extrinsic origin of enhancement of the piezoelectric properties is connected with a change in the population of domains with monoclinic symmetries. The polarization can easily rotate under the electric field's action in such symmetries, to which belong the M_A , M_B , and M_C phases (see the Introduction and Ref. [46]). We have found that rhombohedral domains do not participate in the piezoelectric response.

The data that support the findings of this study are available from the corresponding author upon reasonable request [47].

ACKNOWLEDGMENTS

A.M. appreciates the technical assistance of J. Sobieraj and B. Żmijewski, from the Military University of Technology in Warsaw, during PZT crystallization. This work was supported by the National Science Centre, Poland, Grant No. 2020/37/B/ST3/02015.

The authors declare no conflict of interest.

- [1] G. Binnig and H. Rohrer, *Surf. Sci.* **126**, 236 (1983).
- [2] A. Safari and E. K. Akdogan, *Piezoelectric and Acoustic Materials for Transducer Applications* (Springer Science & Business Media, 2008).
- [3] K. Shung, J. M. Cannata, and Q. F. Zhou, *J. Electroceram.* **19**, 141 (2007).
- [4] X. Hou, S. Zhang, J. Yu, M. Cui, J. He, L. Li, X. Wang, and X. Chou, *Energy Technol.* **8**, 1901242 (2020).
- [5] M. S. Senousy, F. X. Li, D. Mumford, M. Gadala, and R. K. N. D. Rajapakse, *J. Intell. Mater. Syst. Struct.* **20**, 387 (2009).
- [6] E. Sawaguchi, *J. Phys. Soc. Jpn.* **8**, 615 (1953).
- [7] J. Frantti, Y. Fujioka, A. Puzos, Y. Xie, Z. G. Ye, and A. M. Glazer, *J. Appl. Phys.* **113**, 174104 (2013).
- [8] R. G. Burkovsky, Yu. A. Bronwald, A. V. Filimonov, A. I. Rudskoy, D. Chernyshov, A. Bosak, J. Hlinka, X. Long, Z.-G. Ye, and S. B. Vakhruhev, *Phys. Rev. Lett.* **109**, 097603 (2012).
- [9] D. Phelan, X. Long, Y. Xie, Z. G. Ye, A. M. Glazer, H. Yokota, P. A. Thomas, and P. M. Gehring, *Phys. Rev. Lett.* **105**, 207601 (2010).
- [10] A. A. Bokov, X. Long, and Z.-G. Ye, *Phys. Rev. B* **81**, 172103 (2010).
- [11] S. Gorfman, D. S. Keeble, A. M. Glazer, X. Long, Y. Xie, Z. G. Ye, S. Collins, and P. A. Thomas, *Phys. Rev. B* **84**, 020102(R) (2011).
- [12] R. Clarke and R. W. Whatmore, *J. Cryst. Growth* **33**, 29 (2010).
- [13] N. Zhang, H. Yokota, A. M. Glazer, Z. Ren, D. Keen, D. S. Keeble, P. A. Thomas, and Z. G. Ye, *Nat. Commun.* **5**, 5231 (2014).
- [14] D. Vanderbilt and M. H. Cohen, *Phys. Rev. B* **63**, 094108 (2001).
- [15] R. Guo, L. E. Cross, S. E. Park, B. Noheda, D. E. Cox, and G. Shirane, *Phys. Rev. Lett.* **84**, 5423 (2000).
- [16] Z. Wang, N. Zhang, H. Yokota, A. M. Glazer, Y. Yoneda, W. Ren, and Z.-G. Ye, *Appl. Phys. Lett.* **113**, 012901 (2018).
- [17] A. J. Bell, P. M. Shepley, and Y. Li, *Acta Mater.* **195**, 292 (2020).
- [18] S. Gorfman, H. Ch. G. Zhang, N. Zhang, H. Yokota, A. M. Glazer, Y. Xie, V. Dyadkin, D. Chernyshov, and Z.-G. Yee, *J. Appl. Cryst.* **53**, 1039 (2020).
- [19] Y. Xie, Ph.D. thesis, Simon Fraser University, 2013.
- [20] S. Fushimi and T. Ikeda, *J. Am. Ceram. Soc.* **50**, 129 (1967).
- [21] J. Dec, K. Roleder, and K. Stróż, *Solid State Commun.* **99**, 157 (1996).
- [22] A. K. Tagantsev, K. Vaideeswaran, S. B. Vakhruhev, A. V. Filimonov, R. G. Burkovsky, A. Shaganov, D. Andronikova, A. I. Rudskoy, A. Q. R. Baron, H. Uchiyama, D. Chernyshov, A. Bosak, Z. Ujma, K. Roleder, A. Majchrowski, J.-H. Ko, and N. Setter, *Nat. Commun.* **4**, 2229 (2013).
- [23] B. Jaffe, W. Cook, and H. Jaffe, *Piezoelectric Ceramics* (Academic Press, London, 1971).
- [24] B. Noheda, D. E. Cox, G. Shirane, R. Guo, B. Jones, and L. E. Cross, *Phys. Rev. B* **63**, 014103 (2000).
- [25] D. E. Cox, B. Noheda, G. Shirane, Y. Uesu, K. Fujishiro, and Y. Yamada, *Appl. Phys. Lett.* **79**, 400 (2001).
- [26] *IEEE Std. 178-1958 (ANSI C83.23-1960) 1* (1958).
- [27] *IEEE Std. 179-1961 (ANSI C83.24-1962) 1* (1961).
- [28] K. Roleder, I. Franke, A. M. Glazer, P. A. Thomas, S. Miga, and J. Suchanicz, *J. Phys.: Condens. Matter* **14**, 5399 (2002).
- [29] K. Roleder, *J. Phys. E: Sci. Instrum.* **16**, 1157 (1983).
- [30] J. Petzelt, D. Nuzhnyy, V. Bovtun, M. Savinov, M. Kempa, and I. Rychetsky, *Phys. Status Solidi A* **210**, 2259 (2013).
- [31] A. A. Bokov and Z.-G. Ye, *Phys. Rev. B* **65**, 144112 (2002).
- [32] F. Li, S. Zhang, D. Damjanovic, L.-Q. Chen, and T. R. Shrout, *Adv. Funct. Mater.* **28**, 1801504 (2018).
- [33] I. Grinberg and A. M. Rappe, *Phase Transitions* **80**, 351 (2007).
- [34] A. M. Lotonov, V. K. Novik, and N. D. Gavrilova, *Phys. Solid State* **49**, 1330 (2007).
- [35] J. L. Jones, E. Aksel, G. Tutuncu, T.-M. Usher, J. Chen, X. Xing, and A. J. Studer, *Phys. Rev. B* **86**, 024104 (2012).
- [36] See Supplemental Material at <http://link.aps.org/supplemental/10.1103/PhysRevB.105.144104> for details on frequency-dependent Curie-Weiss constants K' and K'' , piezoelectric resonances before and after poling the crystal in a DC electric field, and details of the Metripol technique.
- [37] A. A. Bokov, P. Bajewski, J. Dudek, and M. A. Malicka, *Rocznik Naukowo-Dydaktyczny, Prace Fizyczne (Kraków)* **6**, 55 (1990), <http://rep.up.krakow.pl/xmlui/handle/11716/6520>
- [38] B. Jaffe, R. S. Roth, and S. Marzullo, *J. Appl. Phys.* **25**, 809 (1954).
- [39] D. Phelan, Ch. Stock, J. A. Rodriguez-Rivera, S. Chi, J. Leão, X. Long, Y. Xie, A. A. Bokov, Z.-Guang Ye, P. Ganesh, and P. M. Gehring, *Proc. Natl Acad. Sci.* **111**, 1754 (2014).
- [40] Q. M. Zhang, W. Y. Pan, S. J. Jang, and L. E. Cross, *J. Appl. Phys.* **64**, 6445 (1988).
- [41] F. Li, S. Zhang, Z. Xu, X. Wei, J. Luo, and T. R. Shrout, *J. Appl. Phys.* **108**, 034106 (2010).

- [42] A. M. Glazer, J. G. Lewis, and W. Kaminsky, *Proc. R. Soc. A* **452**, 275 (1996).
- [43] A. Geday, W. Kaminski, J. G. Lewis, and A. M. Glazer, *J. Microsc.* **198**, 1 (2000).
- [44] A. Geday and A. M. Glazer, *J. Phys.: Condens. Matter* **16**, 3303 (2004).
- [45] I. Lazar, A. Majchrowski, D. Kajewski, A. Soszyński, and K. Roleder, *Acta Mater.* **216**, 117129 (2021).
- [46] L. Bellaïche, A. Garcia, and D. Vanderbilt, *Phys. Rev. B* **64**, 060103(R) (2001).
- [47] The data that support the findings of this study are available from the corresponding author upon reasonable request.

Correction: The chemical formulas given in the heading of Sec. IV A and in several locations in text were presented improperly and have been fixed.